SSC19-XI-01

A Year in Space for the CUbesat MULtispectral Observing System: CUMULOS

Dee W. Pack, Christopher M. Coffman, John R. Santiago
The Aerospace Corporation
2310 E. El Segundo Blvd., El Segundo, CA 90245; (310) 336-5645
dee.w.pack@aero.org

ABSTRACT

CUMULOS is a three-camera system flying as a secondary payload on the Integrated Solar Array and Reflectarray Antenna (ISARA) mission with the goals of researching the use of uncooled commercial infrared cameras for Earth remote sensing and demonstrating unique nighttime remote sensing capabilities. Three separate cameras comprise the CUMULOS payload: 1) a visible (VIS) Si CMOS camera, 2) a shortwave infrared (SWIR) InGaAs camera, and 3) a longwave infrared (LWIR) vanadium oxide microbolometer. This paper reviews on-orbit operations during the past year, in-space calibration observations and techniques, and Earth remote sensing highlights from the first year of space operations. CUMULOS operations commenced on 8 June 2018 following the successful completion of the primary ISARA mission. Some of the unique contributions from the CUMULOS payloads include: 1) demonstrating the use of bright stars for on-orbit radiometric calibration of CubeSat payloads, 2) acquisition of science-quality nighttime lights data at 130-m resolution, and 3) operating the first simple Earth observing infrared payloads successfully flown on a CubeSat. Sample remote sensing results include images of: cities at night, ship lights (including fishing vessels), oil industry gas flares, serious wildfires, volcanic activity, and daytime and nighttime clouds. The CUMULOS VIS camera has measured calibrated nightlights imagery of major cities such as Los Angeles, Singapore, Shanghai, Tokyo, Kuwait City, Abu Dhabi, Jeddah, Istanbul, and London at more than 5x the resolution of VIIRS. The utility of these data for measuring light pollution, and mapping urban growth and infrastructure development at higher resolution than VIIRS is being studied, with an emphasis placed on Los Angeles. The "Carr", "Camp" and "Woolsey" fires from the 2018 California fire season were imaged with all three cameras and results highlight the excellent wildfire imaging performance that can be achieved by small sensors. The SWIR camera has exhibited extreme sensitivity to flare and fire hotspots, and was even capable of detecting airglow-illuminated nighttime cloud structures by taking advantage of the strong OH emissions within its 0.9-1.7 micron bandpass. The LWIR microbolometer has proven successful at providing cloud context imagery for our nightlights mapping experiments, can detect very large fires and the brightest flare hotspots, and can also image terrain temperature variation and urban heat islands at 300-m resolution. CUMULOS capabilities show the potential of CubeSats and small sensors to perform several VIIRS-like nighttime mission areas in which wide area coverage can be traded for greater resolution over a smaller field of view. The sensor has been used in collaboration with VIIRS researchers to explore these mission areas and side-by-side results will be presented illustrating the capabilities as well as the limitations of small aperture LEO CubeSat systems.

INTRODUCTION

During the build of the ISARA spacecraft bus it was realized that over 1U of unused spacecraft volume was available in the middle of the 3U spacecraft due to the compact design of the primary JPL/Pumpkin Reflectarray antenna payload and The Aerospace Corporation avionics and bus electronics. JPL offered The Aerospace Corporation the opportunity to fill this payload and following a "no-impact" design study and review, both JPL and NASA approved the addition of a compact remote sensing payload. The CUbesat MULtispectral Observing System (CUMULOS) was built to demonstrate visible nightlights imaging, short-wavelength infrared hotspot and airglow-illuminated cloud imaging, and long-wavelength infrared cloud context imaging and terrain imaging, using low cost, size, weight, and power sensors. Integrating the cameras onto the ISARA mission was a rapid development mission-of-opportunity effort that required the use of immediately available commercial off-the-shelf (COTS) parts, or rapidly modified COTS parts, as well as electronic compatibility with our existing CubeSat camera board hardware[1,2]. To insure the sensors would provide data of interest, we were guided by our experience with nighttime lights and thermal hotspot data from the Defense Meteorological Satellite Program (DMSP) and NOAA's Visible Infrared Imaging Radiometer Suite (VIIRS), as well as by results and data from the Japan Aerospace Exploration Agency's Compact Infrared Camera (CIRC) microbolometer[3-6]. In addition, recent Aerospace Corporation experience imaging the Earth at night with simple utility cameras onboard earlier generation 1- and 1.5-U AeroCube satellites, drove the desire to have a more easily

calibrated monochromatic VIS sensor paired with a LWIR cloud context imager.[7-9] The SWIR sensor was added to investigate airglow cloud imaging in the 0.9-1.7 micron spectral region, where the OH Meinel emissions are strong, as well as to detect fires and flares with good sensitivity. The chosen suite of low-cost night vision cameras allowed a subset of interesting VIIRS-like missions to be addressed over regions of approximately 200km x 150km in a remarkably compact package, and enabled us to explore the performance of uncooled low-cost focal planes and camera cores. Nightlights detection, boat light detection, fire and gas flare detection, and cloud context imaging to better enable the above missions and to investigate microbolometer utility for SmallSat weather missions, were mission goals.[1,2] Three simple wide spectral bandwidth cameras were paired with commercially available fast, compact lenses, and acquired and packaged into less than 1U (10x10x10cm) of CubeSat volume. The CUMULOS was designed to have resolution more than five times greater than VIIRS for the lowlight VIS camera, and similar or slightly higher resolution for the SWIR and LWIR cameras. Sensitivity is achieved through point-and-stare imaging allowing (in the case of the VIS camera) exposures of up to 0.5 seconds to be performed. The sensor choices and ConOps allowed us to perform observations of urban lights and thermal feature mapping, as well as proof-of-concept airglow weather imaging and microbolometer cloud imaging research.

CUMULOS Payload Overview

The CUMULOS payload, ground calibration efforts, mission and spacecraft bus were described in two prior papers[1-2]. The 3-camera flight camera payload and integrated spacecraft engineering model are pictured in figure 1. Basic sensor parameters are summarized in Table 1 below. Parameters, such as camera ground sample distance (GSD), swath and orbital inclination, changed a bit from those planned originally due to the spacecraft being launched into a lower orbit on a different rideshare opportunity than originally planned. The visible camera can be programmed to integrate from 116 µsec to 0.9 sec. This provides enough dynamic range to image morning and evening daytime earth scenes, the full moon, and nighttime lights and clouds illuminated by moonlight (>quarter moon phase). In practice we've typically limited our integration time to 0.5 sec or less and the best city images were taken at 200 or 500msec exposures. Higher gains have been experimented with for some boat light collects. The SWIR camera can be manually programmed to integrate from 185µsec to 31.7msec. Earth images were typically taken at the longest exposure time. The upper 32-msec limit of the integration time is artificially constrained by the nominal 30-hz frame rate of the camera in its intended video mode. Newer versions of this camera do not have this limitation. The SWIR camera has both high- and low-gain settings and both were experimented with for nighttime weather imaging and fire and flare detection. The microbolometer camera is equipped with a shutter. For on-orbit imaging, shutter images are taken right after turn-on and a camera mode is used which uses these to subtract the camera self-emission. Both high and low-gain microbolometer images are taken to provide cloud context and thermal imagery. To date, most of our collections have been single camera frames for a given setting. This is due to the requirement for timely 3-camera images for a given scene (the cameras must be used in sequence) and to our data downlink constraints.

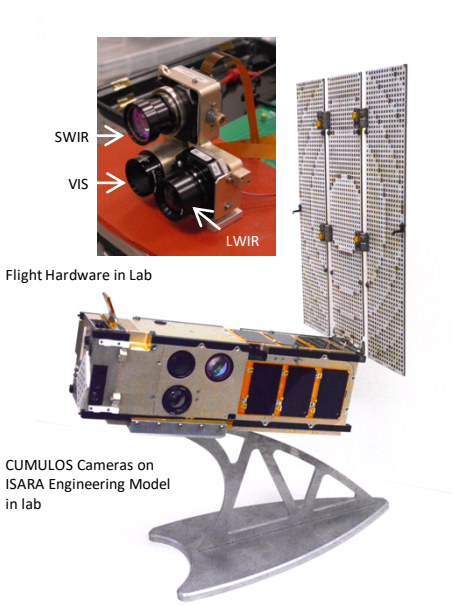

Figure 1. CUMULOS Payload and Engineering Model

Table 1: CUMULOS Sensor Specifications

Sensor Specifications	CUMULOS VIS	CUMULOS SWIR	CUMULOS LWIR
Lens f-number	1.4	1.4	1.1
Lens focal length (mm)	17.6	25	25
Pixel Pitch (µm)	5.2	25	17
Approx. Spectral Band (µm)	0.4 - 0.8	0.9 - 1.7	7.5 - 13.5
Quantization (bits)	10	14	14
Integration time range (msec)	0.116 - 900	0.185 - 31.7	not appl. 10-msec time constant, 30 Hz max
Sensor Vendor Type	Aptina/ON Si CMOS	FLIR InGaAs	FLIR VOx microbolometer
Array Size (pixels)	1280x1024	640x512	640x512
Nominal Alt. (km)	450	450	450
GSD (m)	133	450	306
Approx. Image Footprint (km)	170 x 136	280 x 230	196 x 157

By designing the CUMULOS visible camera with a field of view of approximately 200x150km (the size of a greater metropolitan area), and by utilizing staring imaging to lengthen the amount of exposure time for visible camera focal plane pixels, images greater than 5-times the resolution of current VIIRS day-night-band (DNB) scanning nighttime imaging weather sensors can be collected. These choices, imposed by available focal plane arrays, CubeSat-compatible optics sizing and the desire for a simple sensor, sacrifice area coverage, but deliver decent sensitivity to nighttime emission sources such as human lighting and even moonlit clouds. This allows the CUMULOS sensor to add mission capability for studying nighttime human lighting and other phenomena, and augment the global coverage afforded by the lower resolution, wide-area VIIRS DNB. These types of missions are enabled by the improvement of megapixel-class commercial CMOS imagers in the visible, as well as by mass-produced commercial uncooled 512x640 pixel infrared sensors. Note that the SWIR camera has the largest field of view, the LWIR and the VIS cameras view a smaller collection area.

CUMULOS OPERATIONS

CUMULOS and the ISARA mission were boosted and deployed on 6 December, 2017 by the Cygnus CRS OA-8E mission following its shuttle resupply mission. After the successful conclusion of the primary ISARA mission in early June, 2018, the CUMULOS payload was activated and achieved first light on 11 June, 2018. Since that time over 120 collection experiments have been executed, over 2000 images have been captured and over a Gigabyte of data downloaded. Much of the mission is automated, with operators involved in target selection, imaging plan generation and anomaly resolution. A target list was compiled which included celestial and terrestrial calibration targets, nighttime lights targets such as large urban areas, maritime areas with high ship traffic or concentrations of fishing vessels, active fires, oil industry gas flares, land cover targets including urban heat islands, snow and ice areas, irrigated croplands, coastal littoral regions, and weather phenomena of interest. Figure 2 illustrates the CUMULOS mission cycle.

An Earth-pointed collection experiment begins with operators selecting a target based on location, weather and lighting conditions. Table 2 shows the timeline of an on-orbit image collection experiment. Capturing cloud free imagery of cities was enabled through the use of a weather API and crosschecking with other web-based forecasts prior to tasking. The sequence begins with the satellite nominally tumbling. The attitude determination and control system (ADCS) is initialized only for collection activities. The cameras settings are controlled by sequencing camera register commands to be executed on-orbit. Typically the LWIR camera would take a high and low-gain image, the VIS camera would take a sequence of several integration times and the SWIR camera would take a sequence of auto-mode and manual mode settings of high gain, low gain and integration times. The satellite collects data from the three cameras for approximately one minute. During the image collection period the satellite slews to maintain the boresight vector and approximately 20 images are collected with all three cameras. The mission cadence is limited by ground contact availability and the payload downlink bandwidth. CUMULOS data is transmitted using the 200kbps UHF radio onboard the ISARA spacecraft. An experimental software defined radio offers the potential for increasing the bandwidth by a factor of up to ten times, but has not yet been successfully demonstrated. A five-station RF ground network is currently operated by The Aerospace Corporation with ground terminals in Florida, Texas, Minnesota, California and Hawaii.

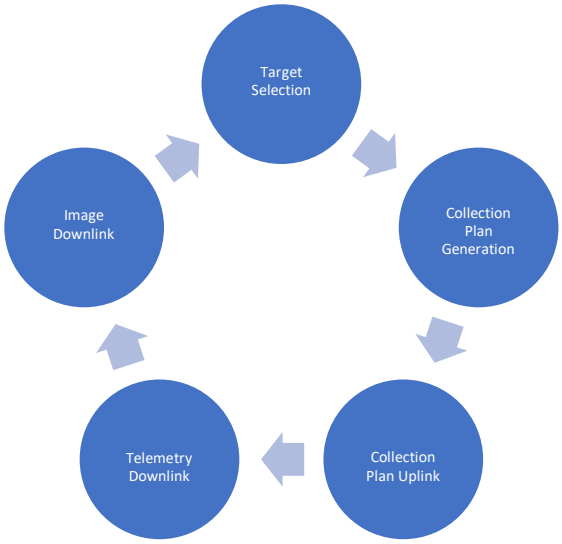

Figure 2. CUMULOS Mission Cycle

Table 2: Collection Timeline

Time	Activity
t - 30 min	System startup
t - 25 min	ADCS initiation
t - 30 sec	Imaging start
t = 0	Minimum range to target
t + 30 sec	Imaging stop
t + 60 sec	ADCS shutdown
t + 4hrs. to 1 day	Ready for next collection activity
t + 3 days	Image downlink complete

Each collection activity requires approximately 2 hours of operator time. Broadly, collection plans fall into three

categories - 1) daytime, 2) nighttime, and 3) celestial with camera settings and star sensor collection geometries appropriate for each category. Once the data is downlinked it enters into a data calibration and georegistration pipeline. Work is still in progress to fully automate the data collection and calibration process and the CUMULOS mission is serving as a testbed for this effort with application to current and future prototype remote sensing flight systems. Our collection plan success rate has improved during the mission as our experience with earth sensor, star camera and attitude determination and control system performance improved for different solar illumination scenarios.

CUMULOS SCIENCE TARGETS

The CUMULOS science target list was divided into a number of different categories: those that enable calibration and sensor studies, and those demonstrate several remote sensing mission areas. These include: stellar, lunar and terrestrial calibration targets, a cities list (for urban geography, growth and change monitoring, light pollution, natural disaster response), severe storms and other weather phenomena, fishing boat areas and other maritime targets, interesting geographical features, and selected satellite conjunction targets (VIIRS - CUMULOS same time collection, often weather-focused).

Stellar Calibration Targets

The proper use of stellar calibration sources has been an area of study by Aerospace Corporation astronomers for 20 years or more.[10-12] We utilize existing stellar models, validated by recent calibrated spectroscopic measurements at astronomical observatories, as our on-orbit calibration standards. The stars chosen initially were αTau (Aldebaran), αLyra (Vega), αBoo (Arcturus), αCMa (Sirius). These stars are bright in both the visible and the short-wavelength infrared and are stable calibration stars, or well-understood and recently measured, as in the case of αTau. Sun-like G-class stars were also considered as calibration targets to reduce the complexity in comparing our results to the solar-diffuser-derived calibration of the VIIRS DNB. The Sun-like stars that were initially selected proved too dim for us to easily use as calibrators with our small aperture CubeSat cameras. Dark sky targets for dark frame measurements included the north and south galactic poles and the Lockman hole. Star measurements were also used for VIS and SWIR sensor boresight determination, an important step for accurate georegistration.

The Moon

We take periodic on-orbit observations of the moon at various phases for varying gain and exposure settings using all three CUMULOS cameras. The goal is to gain experience with the use of the empirical USGS Robotic Lunar Observatory (ROLO) model of lunar irradiance.[13,14] The ROLO model covers 0.35-2.5 microns a range that spans our broadband VIS and SWIR cameras. Comparing results of lunar calibration to stellar calibration is one of our goals, as is the comparison of these results to ground target measurements. We also have used lunar measurements to validate our ground-based flat-field observations. The Moon was also the only celestial target that could be observed by all three sensors in common.

Terrestrial Calibration Targets

We chose a list of psuedo-invarient ground calibration sites for daytime reflectance calibration, but have not yet taken frequent measurements on these sites, primarily due to our focus on calibrating the nighttime performance of our VIS and SWIR cameras. The sites chosen are from the LANDSAT test site catalogue.[15] We have started taking measurements of standard thermal radiometric calibration sites used to calibrate the Landsat-8 TIRS and other sensors. Lake Tahoe was the first target selected, and offers a large-area, high altitude, known emissivity, instrumented, uniform LWIR calibration target. Data on this site from multiple lake surface temperature buoys, radiometers and other instruments are published by JPL.[16]

Urban Targets

Cities chosen for study by the CUMULOS sensors were selected based on size, weather, and coastal proximity. This insured multiple remote sensing phenomenology interest areas could be serviced by one urban imaging experiment. Some of these multi-phenomenology examples will be presented in the thermal sources and weather sections below. All nightlight studies depend on laying down a baseline of data, so our initial cities were chosen to be of general interest to the nighttime lights research community. CUMULOS city data can also be used to better understand the capabilities and limitations of existing VIRSS DNB and DMSP Operational Line Scanner (OLS) data sets and advanced processing techniques. Cities for which imaging experiments have been performed to date include: Abu Dhabi, Baghdad, Hongkong, Istanbul, Jakarta, Jeddah, Kuwait City, Los Angeles, London, Shanghai, Singapore, and Tokyo. Several of these have been imaged multiple times. Weather impacted some collects, making the data more useful for the study of clouds. Many other attempted collections on other cities failed during the time period in which the engineering team was tuning the ADCS pointing, the use of several earth-sensors, and star sensor stray light thresholds.

Fires, Gas Flares and Industrial Hotspots

The CUMULOS team made an effort to image a number of the severe wildfires that occurred during 2018. The California "Carr", "Camp" and "Woolsey" fires were imaged successfully. Natural gas flares are another subject of interest for remote sensing study for multiple environmental science and economic reasons.[3,17,18] Bright flares are also potentially useful as terrestrial point sources for sensor boresight confirmation and georegistration accuracy assessment. Imaging the cities of the Persian Gulf region in Kuwait and the UAE also exhibited a large number of terrestrial and offshore flares, as did Jakarta, Los Angeles and other regions. Other types of flares and industrial hotspots show up in CUMULOS imagery of cities, particularly the SWIR camera.

Maritime Domain Awareness

Fishing boats are brightly lit at night and are routinely detected by the VIIRS DNB, as are other types of more dimly lit vessels.[19] CUMULOS was tasked to look at areas known to have large numbers of fishing boats, or other concentrations of shipping such as well-traveled shipping lanes. Sites observed with dense ship concentrations included the Java Sea and the Gulf of Oman. Sites were selected in collaboration with Dr. Chris Elvidge's team who create the VIIRS DNB nightly "boat lights" product.[19] The goal is to determine how well a CubeSat can perform this mission and to assess VIIRS performance at detecting densely concentrated ships that can be more easily resolved by our higher resolution CUMULOS VIS camera. Ship lights also appeared in many of our other images of coastal cities.

Weather Targets

CUMULOS weather targets include: airglow illuminated clouds, severe storms, sea ice, snow-covered terrain and complex cloud scenes in general. A series of on-going conjunction collects between CUMULOS and the VIIRS sensors onboard the Suomi-NPP and JPS-1 satellites, are being performed in collaboration with a team at the Colorado State University Cooperative Institute for Research in the Atmosphere (CIRA) led by Dr. Steven Miller. Goals for this effort include assessing CUMULOS calibration via comparison to the well-calibrated VIIRS sensor, studying the performance of the CUMULOS microbolometer, and comparing the ability of the broadband CUMULOS SWIR camera for airglow imaging of clouds to that of the VIIRS DNB. Demonstrating imaging of clouds at night illuminated by airglow only under zero moonlight conditions was one of the primary remote sensing goal for CUMULOS. We tasked several experiments during new moon with this goal in mind, as well as several conjunction experiments with VIIRS. Additional weather targets are high cold clouds for assessing microbolometer performance. We made an effort to image tropical cyclones during the 2018 hurricane season. Storms on which data were collected included: Lane, Soulik, Rosa, Willa and Yutu.

Other Terrestrial Targets

Sites with strong thermal contrast signals are of interest, including: land/sea interfaces and littoral regions, urban heat islands and irrigated fields. Some of these overlap with weather imaging interests and include glaciers and snow covered landscapes, sea ice.

Special Experiments - Laser targeting

The CUMULOS SWIR camera has been used recently as a receiver for laser crosslink demonstrations from space-based CubeSats operated by The Aerospace Corporation. Ground-based lasers are also planning to use the CUMULOS cameras as test receivers for ground to LEO spacecraft pointing experiments. The wide 0.9-1.7μm band pass make the InGaAs camera a convenient on-orbit laser receiver asset for these tests. The space experiments are described in a paper by Welle.[20]

CUMULOS CELESTIAL OBSERVATIONS

Observations of stars, the Moon and Mars were taken initially for boresight and focus checks, and then later and more carefully to obtain stellar and lunar calibration data. CUMULOS had a basic boresight check performed in the laboratory on a hot emission point target and laboratory scenes. For initial on-orbit boresight determination, observations were performed on the Moon (visible to all three sensors), and selected bright stars (visible only to the VIS and SWIR cameras) The stars selected were chosen to also be useful for radiometric calibration. We used stellar observations of alpha Tau for accurate VIS and SWIR camera boresight correction. The VIS camera was able to take unsaturated lunar data for some of its settings, as was the LWIR microbolometer. Unsaturated lunar data were used to assess the ground test flat field data, and were also set aside for applying the USGS ROLO model for calibration purposes. The SWIR sensor saturated on the full moon and we were unable to manually program it to take unsaturated data, despite its auto-modes being capable of taking unsaturated Earth scenes. (The auto-modes attempts to boost the integration time and gain for the space scenes since the majority of the frame is dark). Only the register settings needed for nighttime imaging were well-documented enough to be programmed manually by our engineering team. This limitation meant we could only calibrate the SWIR camera for nighttime use. This wasn't a major hindrance since our research goals for this camera mainly involved stellar calibration, nighttime hotspot measurements and nighttime imaging of clouds illuminated by airglow and moonlight.

Stellar Calibration sources: alpha Tau and alpha Lyra

We chose the two stars, alpha Tau and alpha Lyra, for a series of initial observations to radiometrically calibrate the CUMULOS VIS and SWIR cameras. Stellar spectral flux models were provided by Dr. Richard Rudy of the Aerospace Corporation.[21] Two stellar models are plotted below in figure 3 along with the solar spectrum for comparison. Alpha Lyra is a hotter star than the sun, and alpha Tau is a cooler star. For both cameras, a sweep of exposure times and gains settings were taken to match and span those used in Earth observation. Data were then dark corrected and flat-fielded using ground test-derived dark correction and flat field files. Example data is shown below from the VIS camera in figure 4. For the SWIR sensor dithered observations of the stars were performed and the frame pairs were subtracted instead of using ground-based dark measurements. This was necessary to correct for hot pixels which appear in our on-orbit data from the InGaAs focal plane. The stellar radiance signals were integrated within a stellar sampling box, and an outer annulus was integrated and subtracted to remove the residual background. Typical integration box dimensions were 17x17 and 31x31 pixels for the VIS camera and 9x9 and 17x17 pixels for the SWIR camera. Results of these flux measurements are plotted in figures 5 and 6.

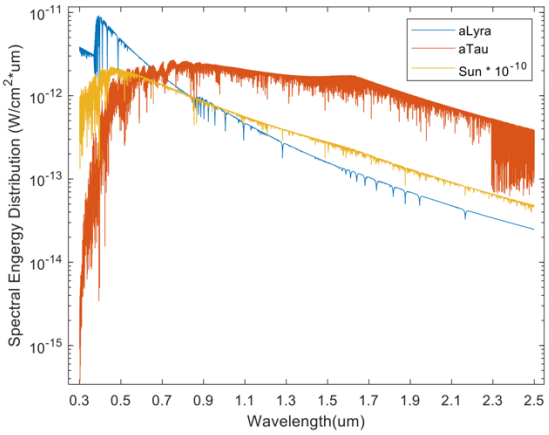

Figure 3. Stellar flux models for alpha Tau and alpha Lyra compared to the Sun.

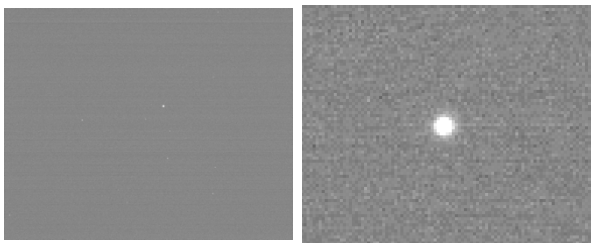

Figure 4. Example full frame and detail of a VIS camera star observation (50msec exposure of calibration star alpha Lyra).

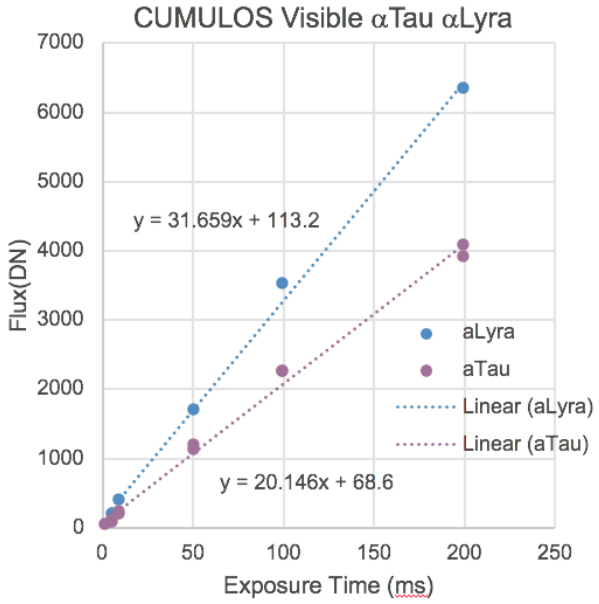

Figure 5. VIS Camera Stellar Calibration Data.

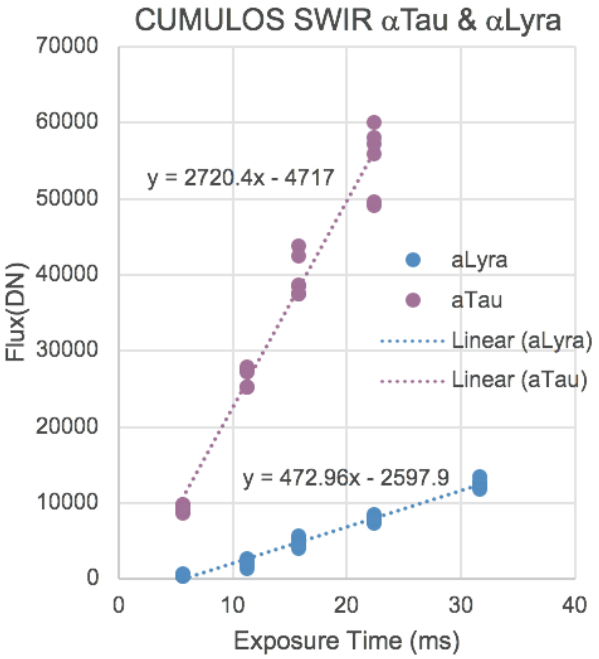

Figure 6. SWIR Camera Stellar Calibration Data

The fits plotted in figures 5 and 6 assume a linear calibration function. We may refine this as more data are obtained and detailed comparisons to ground calibration results are carried out. To complete the calibration the measured signals or slopes are converted from digital number (DN), or DN-msec^{-1}, to W-cm^{-2} using the stellar spectral energy flux model. We account for the quantum efficiency of the VIS and SWIR focal plane detectors

and the transmission of the lenses used. There are no filters on these cameras. The equation is:

$$Flux = \frac{\int \mathrm{SE}(\lambda) QE(\lambda) T(\lambda) d\lambda}{\int QE(\lambda) T(\lambda) d\lambda} \quad (1)$$

for spectral energy distribution, SE, quantum efficiency, QE, and transmission, T. We divide by the two camera's per pixel solid angles to convert these results into W-cm^{-2}-sr^{-1}. To accurately compare results from the two stars we also convert to photons-s^{-1}-cm-^{2}-sr^{-1}, which is the proper way of comparing signals from two sources that differ spectrally since the cameras respond to the numbers of photons, not the energy. The results from the stellar calibration are tabulated for the two cameras in Table 3.

Table 3: CUMULOS Camera Calibration

Sensor/ Star	DN/msec	W-cm^{-2}-sr^{-1}	ph-sec^{-1}-cm^{-2}-sr^{-1}
VIS/αTau	1	9.379x10^{-7}	3.156x10^{12}
VIS/αLyra	1	1.119x10^{-6}	3.067x10^{12}
SWIR/αTau	1	6.514x10^{-10}	4.171x10^{9}
SWIR/αLyra	1	6.850x10^{-10}	4.033x10^{9}

The agreement between the stellar measurements of alpha Tau and alpha Lyra is excellent: 2.9% for the VIS camera results and 3.4% for the SWIR camera. We intend to continue measuring additional bright calibration stars, for which we have accurate, data-anchored models, and to refine the accuracy of our calibration process as applied to CUMULOS and other small CubeSat cameras. We are guided in this effort by the detailed body of work of Russell and co-workers on the accurate use of stars as space sensor calibration targets.[10-12] It is hoped that via careful, well-understood cross-calibration, our data can be compared in detail to VIIRS DNB data. An accounting will have to be made for the differences in the calibration sources used by the two sensors (solar diffuser vs. selected bright stars) and relative spectral responses. Our conjunction experiments will assist with this when analyzed in detail, as will careful study of well-understood isolated point sources.

URBAN IMAGING: CITIES AT NIGHT

DMSP OLS and VIIRS DNB imagery are powerful tools for monitoring human development and the human footprint on Earth.[5] These sensors have been used to study human lighting at night for a variety of purposes. These include: mapping light pollution, mapping urban and suburban growth and transportation grids, studying national, regional and municipal energy usage and correlated economic activity, measuring the growth of developing nation's power grids, and mapping post-disaster loss and recovery of power grids. It was the aim of the "nightsat mission concept" to develop a smallsat to address the need to measure nighttime lights at higher resolution, with 20-50 meters as a goal.[22] The CUMULOS VIS camera is a compromise design in a CubeSat form with a GSD of 130 meters, and a large enough field of view to study cities and very small countries in a single image. The resolution is a factor of 5.6 improvement over the 740-m resolution of the VIIRS DNB. As a "flying camera" capability in ISS orbital inclination, CUMULOS is similar to ISS nighttime photography.[23,24] As a free-flying space sensor, CUMULOS is able to image on demand, however, and point freely at stellar and lunar calibration targets for unambiguous on-orbit calibration. The LWIR microbolometer also contributes to the urban imaging mission by providing same-time cloud context imagery for selecting cloud-free data. The SWIR camera adds additional information on industrial hotspots from flares and other hot emission sources. This synergy between cameras also holds for wildfire observations and weather studies presented later.

Nighttime Imagery of Los Angeles

Los Angeles has been an initial focus of our nighttime remote sensing studies. Our goals are to characterize the regional light emissions and to baseline our CubeSat nighttime lights capabilities for monitoring light pollution at the urban-wildlands-coastal boundaries. The CUMULOS data are currently the highest resolution calibrated nightlights product available for this type of research effort. Understanding these data and using the lessons learned to help build better sensors for future weather or nightlights missions is a goal. Figure 7 shows a 200msec exposure image of Los Angeles. When imaging cities we take a range of exposures, with 200-500msec typically providing the best results. A number of features are labeled in figure 7. The data are logarithmically stretched to highlight both the urban grid and lights from less developed neighborhoods as well as point targets such as ship lights and offshore platforms. Our initial series of images of Los Angeles were taken on the nights of 2018 Oct. 7, 12 and Nov. 13 and allows us to perform some time series comparisons, comparing cloudy vs. cloud-free nights, and also showing the impact on the power grid of the Woolsey fire which impacted the Malibu region. These additional data will be documented in the slide presentation that accompanies this paper. Other targets of interest appear in these related data sets. Our calibrations show we can detect signals as low as 4-8 nw-cm^{-1}-sr^{-1} at typical VIS camera exposure times and noise levels. Empirical comparison to VIIRS DNB suggest we may be able detect signals of 2 nw-cm^{-1}-sr^{-1} as measured by the VIIRS DNB calibration. We will be refining these comparisons as our calibration matures, as conjunction

data with VIIRS gets analyzed, and as we reconcile the two sensors different wavebands and calibrations.

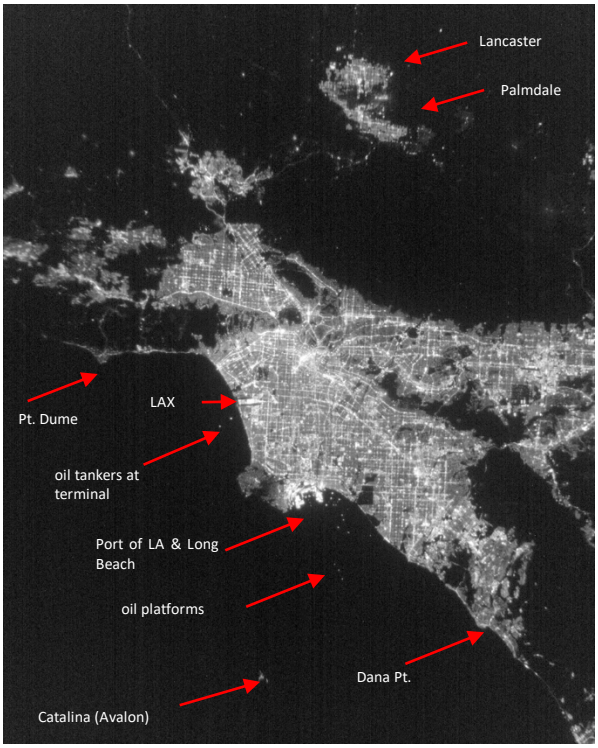

Figure 7. Los Angeles Imaged by the CUMULOS VIS Camera 2018 Oct 12, 05:05 UT. No Moonlight.

Figure 8 shows the corresponding SWIR and LWIR camera images. The SWIR image shows extensive urban signals in the 0.9-1.7micron waveband, but does not map the urban grid as accurately due to its 450-m resolution.

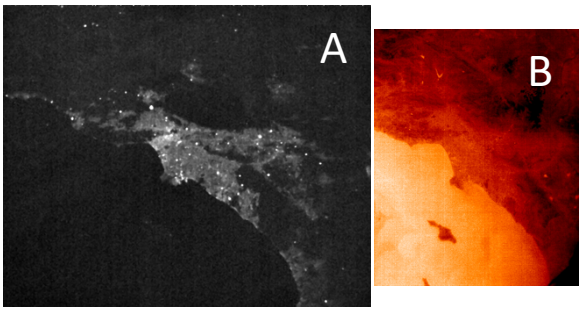

Figure 8. Los Angeles Imaged by the CUMULOS A) SWIR and B) LWIR Cameras. No Moonlight.

Notable SWIR features include hotspots scattered around the region. Some of these are from readily identifiable gas flares, but many others are co-located with landfills and are likely to also be from low-level methane flaring. The LWIR microbolometer image provides cloud context and shows the lack of cloud cover over the Los Angeles metropolitan area. Thermal features from terrain, land-water contrast, including that from a number of warm brightness temperature reservoirs, are evident as are subtle ocean temperature variations. VIIRS DNB data are shown in Figure 9 for comparison. There is no lunar illumination.

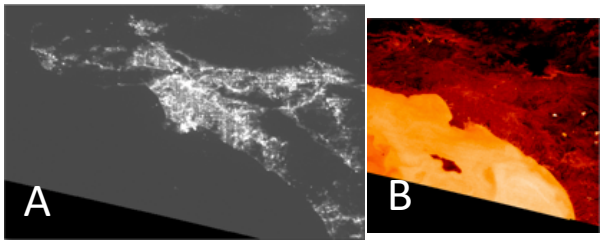

Figure 9. VIIRS DNB Data of Los Angeles 2018 Oct 12 10:11 UT. A) DNB, B) I-5 (10.5-12.4 µm)

Two Asian Mega-Cities: Shanghai and Tokyo

Figure 10 shows nighttime data from greater Shanghai and Tokyo side-by-side, major cities with regional populations of 26 million and 38 million people, respectively. A logarithmic stretch is applied to the data to better display the full dynamic range of these nighttime images. Infrastructure such as bridges, roads, airports, rail networks, and refinery flares stand out, as well as subtler lights from ships moored in the Yangtse River and Tokyo Harbor, and dim lights in more remote areas surrounding these two huge cities. Shanghai features include: A) Shanghai Hongqiao Railway Station & International Airport, B) Sutong Changjiang Highway Bridge, C) Chongqi Changjiang Highway Bridge, D) Shanghai Changjiang Bridge, E) Shanghai Pudong International Airport, F) Donghai Bridge, G)Yangshan Deep Water Port, H) Hangzhou Bay Bridge. Notable dark areas include the mouth of the Yangtse River, the Huangpu River bisecting Shanghai and Pudong, and Hangzhou Bay. Tokyo features include: A) Yokohama Harbor, B) Haneda International Airport, C) Tokyo Harbor, D) JFE Chiba Steel Work, E) Tokyo Bay Aqua-Line bridge/tunnel, F) Chūō Line rapid service rail line showing linear evenly spaced stations, and G) Narita International Airport. Notable dark areas include: Tokyo Bay, though it is full of numerous ship lights and a hint of illuminated haze, Sagami Bay, the Tanzawa Mountain forests west of Tokyo, and the Bōsō Peninsula which forms the eastern edge of Tokyo Bay. The images were both taken at 500msec exposures.

Interpretation of the VIS camera nightlights data is enhanced by using the thermal and short-wave infrared imagery from the other two camera payloads. Figure 11 shows data from the LWIR microbolometer and SWIR camera for Shanghai. The LWIR camera unambiguously shows the city center is cloud-free with obvious cloud structure far to the north. Other striking thermal features are the Haungpu River bisecting the Shanghai, various lakes, the urban heat island, temperature variations in the river delta zone, and numerous subtle inland canal

features. The high gain SWIR image shows waste light in the .9-1.7 micron bandpass from urban lights, bright features from industrial thermal sources such as refinery flares and also images the clouds to the north and east. The moon is at 52.1°elevation, 177° azimuth, 32% illuminated for the Shanghai imagery. The moon was only 3% illuminated and below the horizon for the Tokyo imagery.

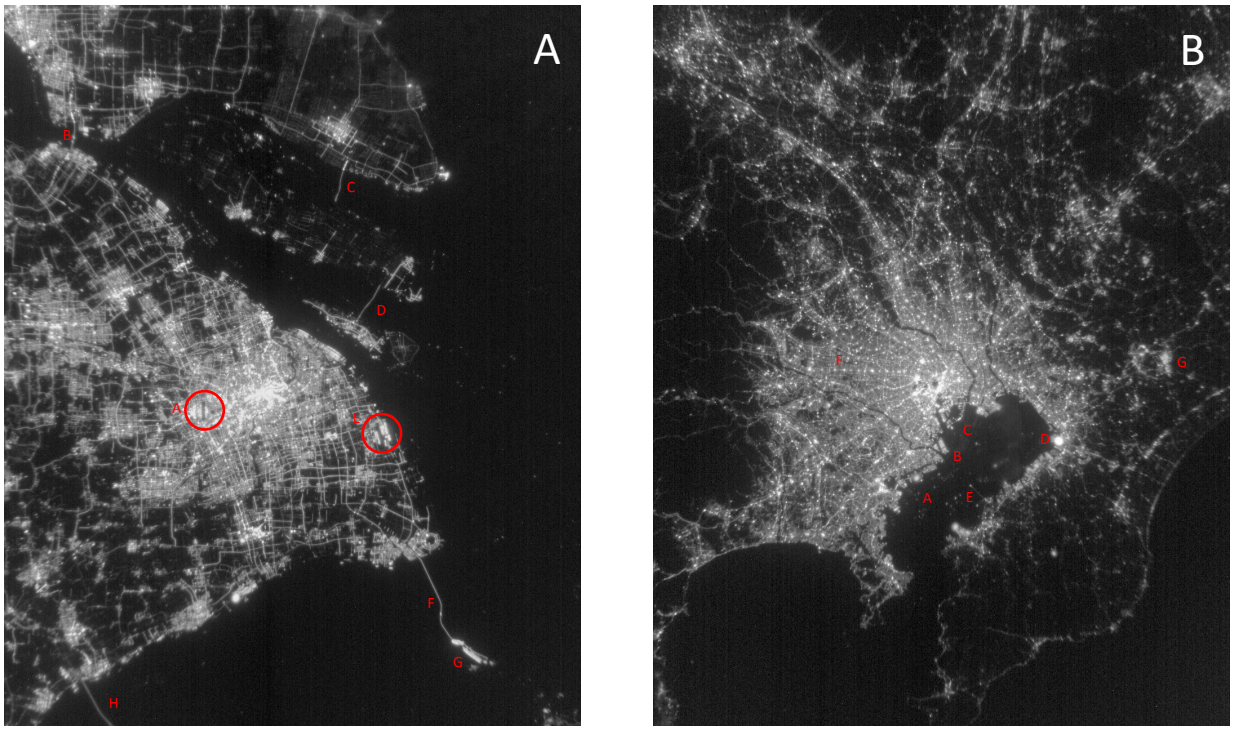

Figure 10. Two Asian Mega-Cities Imaged by the CUMULOS VIS camera. A. Shanghai, 2018 December 13, 12:50 UT, 0.5 second exposure. B. Tokyo, 2019 February 6, 13:42 UT, 0.5 second exposure.

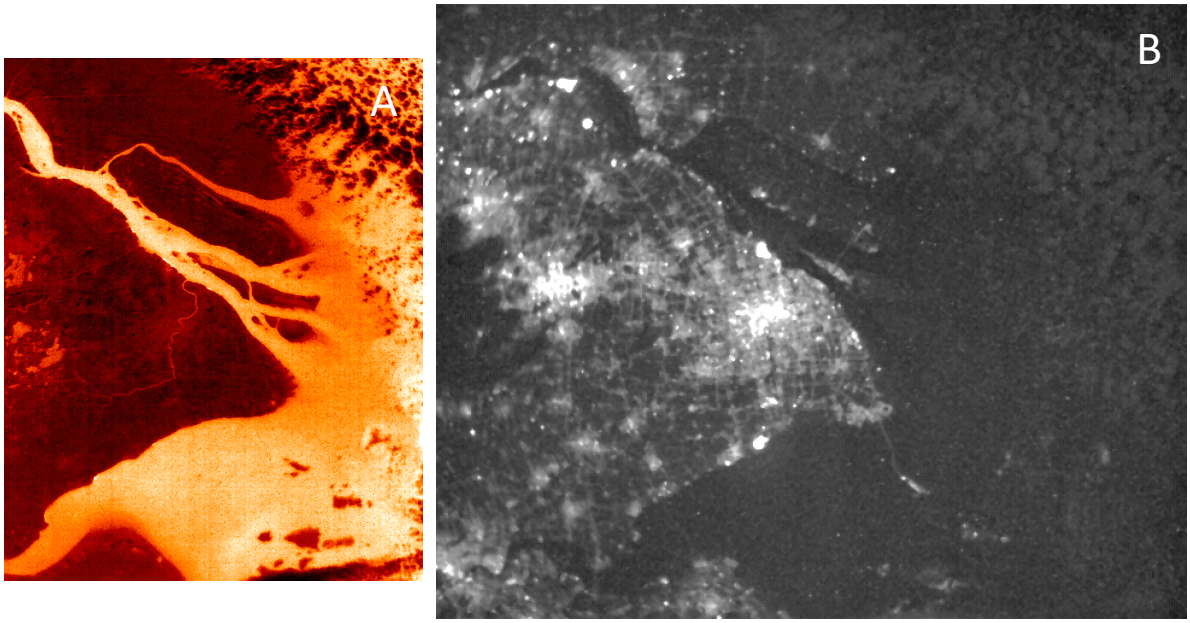

Figure 11. Shanghai imaged by the CUMULOS LWIR microbolometer and SWIR cameras on 2018 December 13, 12:50 UT. Both cameras are in high gain mode, the SWIR image has a logarithmic stretch applied. The SWIR camera is exposed for 31.7msec.

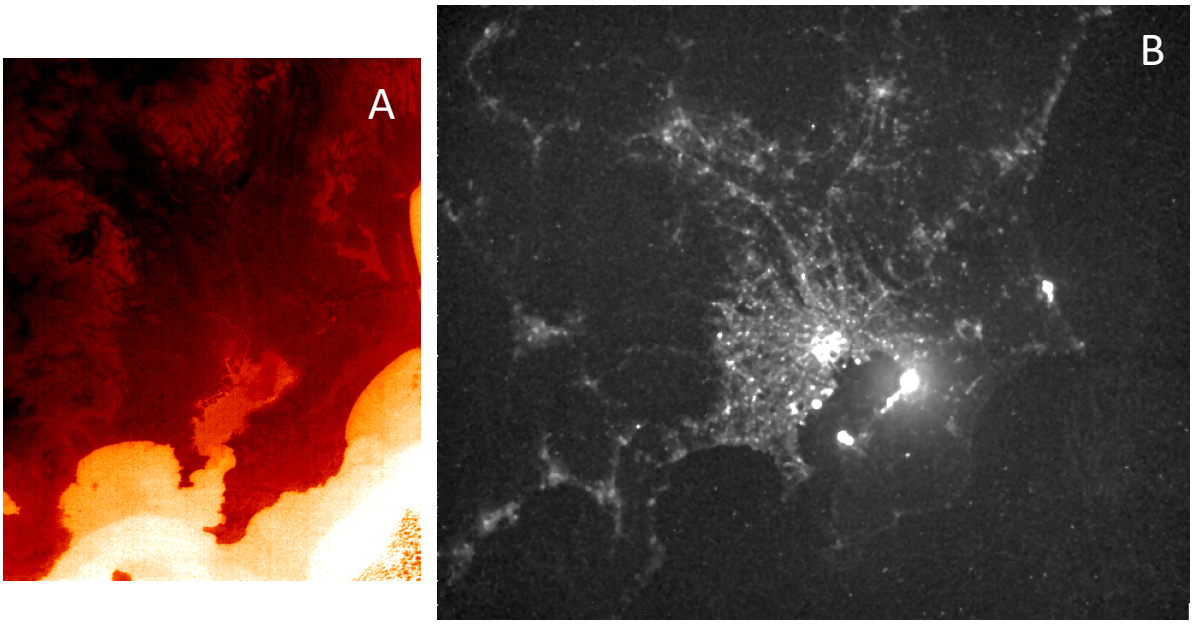

Figure 12. Tokyo imaged by the CUMULOS LWIR microbolometer and SWIR cameras. 2019 February 6, 13:42 UT. No lunar illumination.

The complimentary LWIR and SWIR images of Tokyo are depicted in figure 12. Again, conditions are totally cloud free over the urban area we wish to study. The microbolometer provides excellent thermal context imagery and shows only a small area of scattered clouds out to sea to the southeast of Tokyo and possible haze over Tokyo Harbor. River and lake features appear, as do subtle variations in coastal water temperature. Bright thermal features from a handful of industrial areas are evident in the LWIR only with heavy stretching of the image histogram. The SWIR camera image exhibited saturation in high gain mode on a number of industrial hotspot regions along the edge of Tokyo bay, and on a large refinery complex on the eastern coast of Honshu. The Bōsō peninsula exhibits a notable SWIR hotspot in its otherwise dark center seen in common with the VIS camera. This is possibly from a greenhouse complex. Low warm, clouds are detected in the LWIR over the ocean to the southeast of Honshu, but do not show a strong signal in the SWIR. Other very low signal-to-noise ratio clouds to the east of Honshu barely appear in the SWIR. These example Shanghai and Tokyo imagery show the power of CubeSat-sized sensor systems to provide nightlights, and supporting infrared data over a large urban region. The three sensors work together as envisioned, with the monochromatic VIS camera providing 130-m GSD nightlights, the SWIR data highlighting hot emission sources, and the LWIR data providing thermal cloud cover and terrestrial thermal imagery. When our data pipeline is finalized, these and other examples will be made available with the radiometric calibration applied (for the VIS and SWIR initially), and in georegistered formats. Our goal is not only to provide research quality nightlights data, for the variety of research purposes already discussed, but to develop the process for building, flying and calibrating small spacecraft for follow-on efforts to craft a viable future "NightCube" mission in the spirit of the "Nightsat Mission Concept" paper outlined originally by Elvidge and coworkers.[22] As we will show in the following section, small staring sensors of the type demonstrated by CUMULOS not only have nightlight mission capabilities, but wildfire monitoring capabilities as well.

WILDFIRE OBSERVATIONS

The 2018 wildfire season in California had a number of particularly disastrous fires. CUMULOS successfully observed three, the "Carr", "Camp" and "Woolsey Fires". Both the "Carr" and "Camp" fires were observed when they were near their worst conditions. The Woolsey fire was observed after the worst of the conflagration, but showed the impact on the power grid, as well as residual hotspot activity. Figure 13 shows nighttime imagery from the CUMULOS cameras on the "Camp" fire that destroyed the town of Paradise, CA. The SWIR image is a composite of the high- and low-gain images. The three cameras together provide complimentary imagery of the wildfire disaster area with the visible camera detecting the fire emissions and nightlights from nearby communities, the SWIR camera providing the most sensitive measurements of the extent of the fire line, and the LWIR camera detecting the hottest parts of the fire line and providing terrain context

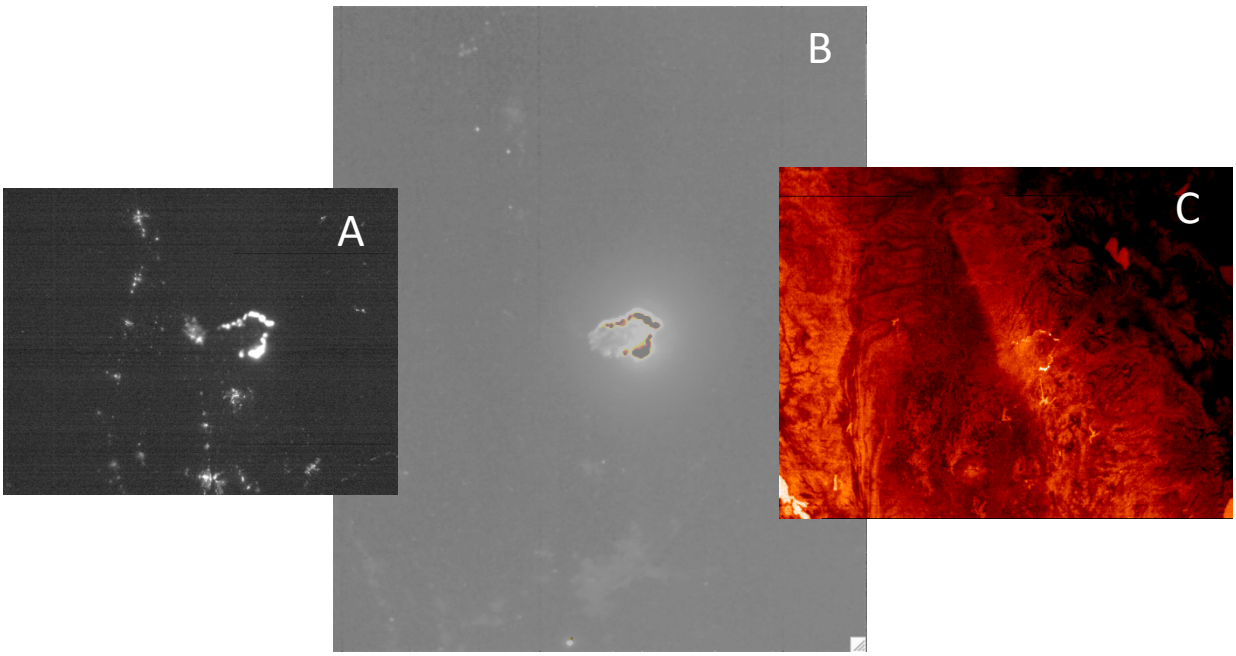

Figure 13. The "Camp" fire imaged by CUMULOS 2018 Nov. 10, 10:48 UT. A) VIS camera data showing the nighlights of Chico, CA and other communities west of the fire. B) SWIR camera high and low gain composite image. Waste light from Sacramento visible to the south shows the huge extent of the "Camp" fire. C) LWIR camera. The fire line is clearly seen in the microbolometer data and contains the hottest pixels in the scene. Thermal features from are also prominent as are thermal features from terrain features

imagery. The pattern of the fire line very closely matches that measured by MODIS.[25,26] CUMULOS results show that building a nighttime-capable fire satellite in CubeSat form is quite possible. To improve overall mission utility and sensitivity, a more capable daytime capability will be desirable to add, either via a MWIR camera, a less solar sensitive SWIR band, or a higher resolution LWIR camera. Explorations of this type are planned for a CUMULOS follow-on study effort, termed AltoCUMULOS, for Advanced CUbesat MULtispectral Observing System.

GEOREGISTRATION EXAMPLE: KUWAIT CITY AND NATURAL GAS FLARES

Some of the brightest repeatable point source light emitters on Earth are those from large natural gas flares complexes. These make useful fiducial sources for understanding spacecraft sensor boresighting and georegistration accuracy. VIIRS researchers have recently catalogued these emission sources, performed multi-band radiometry on them, and created a useful global map that characterizes global oil industry natural gas flaring activity.[17,18] We wanted to point CUMULOS at a number of these sites and study sensor performance as well as exploit the measured locations of the flare stacks for georegistration purposes. Figure 14 shows georegistered CUMULOS VIS, SWIR and LWIR data of the Kuwait-Iraq border region which has a number of very bright emissions sources. The Moon was at 12.5° elevation, 236.6° azimuth, and 58% illuminated when these images were taken, and no clouds are evident. The Rumaila gas-oil separation plant flares in southern Iraq appear strikingly in the SWIR imagery. The pushpin and gas pump symbols on the maps mark the VIIRS-measured locations of the known frequently observed flare emission sources. Correlating our CUMULOS data with these sites as well as lights from road grids, urban regions for the VIS and SWIR cameras, and land-sea coastal boundaries in the LWIR, allows us to test the accuracy of our autogeoregistration data pipeline. Currently we can georegister data to about 2 pixel accuracy for the VIS and SWIR imagery and are working to improve this and correct the boresight of the LWIR camera to bring its accuracy into line as well.

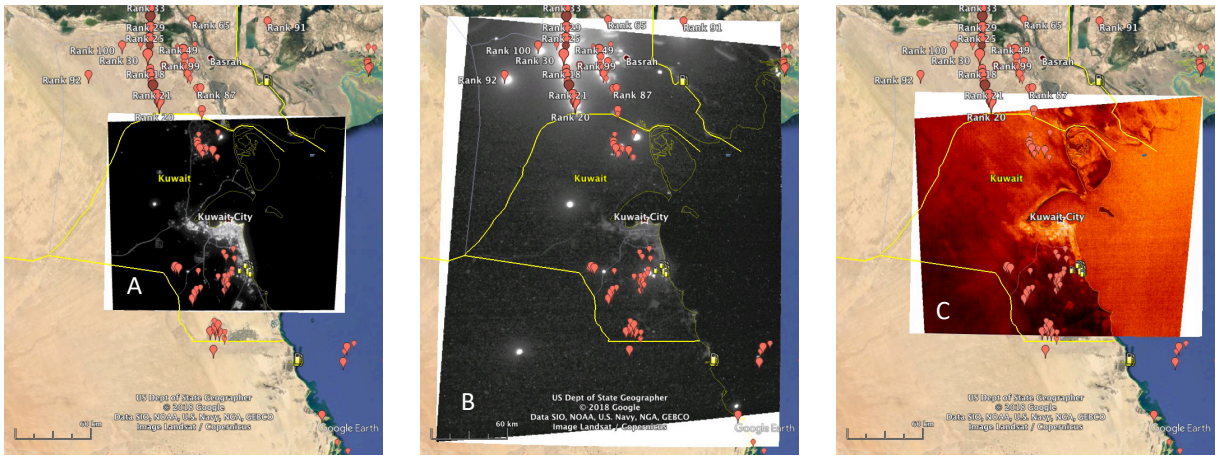

Figure 14. Georegistered CUMULOS data of Kuwait 2018 Sep. 17, 19:19 UT. Left to right A) VIS, B) SWIR and C) LWIR data. Coastal regions with very bright gas flares, road grids and urban regions are excellent tests of georegistration accuracy.

MARITIME DOMAIN AWARENESS

Lights from shipping are routinely observed by DMSP OLS and the VIIRS DNB, particularly the bright lights from fishing vessels which attract fish at night with intense illumination of the ocean surface. VIIRS DNB data are being used by Elvidge and coworkers to generate boat detection products which are being assessed for fisheries management.[19,27] Dense concentrations of illuminated vessels can pose a challenge for detection and counting by the VIIRS DNB sensor which has a GSD of 740-m. Figure 15 shows CUMULOS VIS camera data of the coastal border region of the United Arab Emirates and Oman and a map of the region imaged. The data are stretched to enhance the boat light detections. The moon was down at the time of the CUMULOS overpass (moonset was at 19:12 UT). A closely spaced concentration of moored, illuminated vessels, most likely brightly lit oil tankers, are evident off the coast of the port of Fujairah. Another cluster of lights appear to the northeast in the Gulf of Oman just outside the strait of Hormuz as well as other scattered lights from ships at sea. The brightly lit coastal cities appear along with the well-lit highways. A bright signal on the southern coast from an Omani refinery flare appears in all three cameras. Figure 16 shows the corresponding CUMULOS LWIR and SWIR imagery whose larger fields of view touch the Iranian coast. The LWIR shows cloud free conditions on the eastern coast of the UAE and Oman and cooler temperatures at higher elevations inland and possible clouds on the western edge of the image. A thermal source is evident on the coast of Oman co-located with a refinery flare complex. The SWIR camera, tasked in high gain mode, captures the lights from Dubai on the western side of the image, as well as from inland cities on the border of the UAE and Oman, within its larger field of view. It also (barely) detects the ship lights, the coast of Iran and possible low cloud features over the Gulf of Oman (the latter features illuminated by airglow only). There is a stray light artifact in the upper left of the image. We've seen this lens artifact in other images of the Persian Gulf region with very bright emission sources in or near the sensor field of view.

Other ship light observation experiments have included fishing boat concentrations in the Java Sea[26], and ships in the Singapore strait, the latter case shown below in the CUMULOS weather observations section.

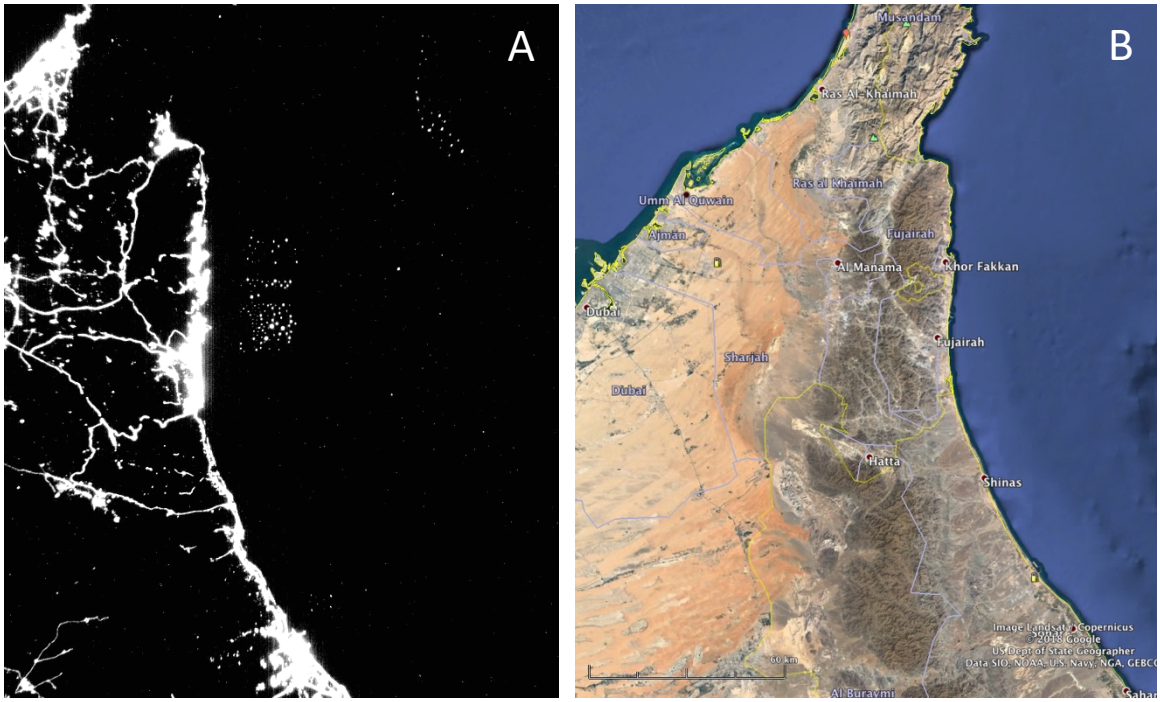

Figure 15. A) Ships moored off the UAE imaged by the CUMULOS VIS camera 2019 May 9, 22:45 UT. B) Map of region imaged.

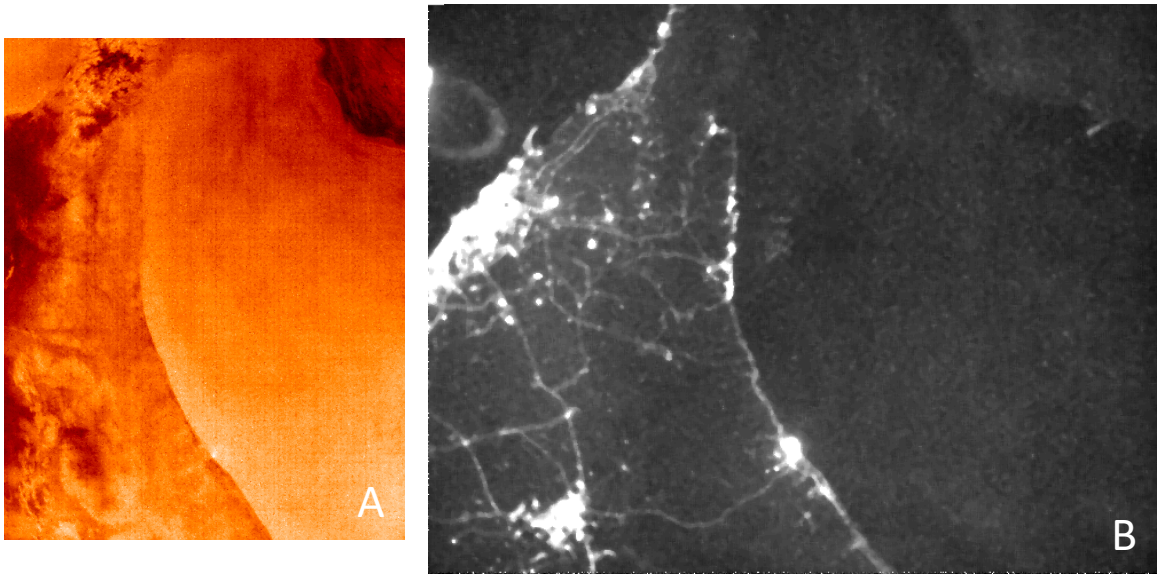

Figure 16. Coastal UAE and Oman imaged by CUMULOS 2019 May 9, 22:45 UT. A) LWIR microbolometer, B) SWIR camera.

CUMULOS WEATHER OBSERVATIONS

We next present a few of our nighttime weather observations, which are also rich in other types of phenomena such as city lights, boats, offshore flares, even an active volcano. We also show new Moon observations of airglow illuminated clouds, including one taken during a VIIRS conjunction. A twilight image of the eye of a tropical cyclone (Hurricane Willa) is also presented.

Singapore - Moonlit clouds, city lights, ship lights

Singapore exibits dynamic weather with much thunderstorm activity. Figures 17- 20 show the city state partly enshrouded in clouds, but with some of the city center visible along with moored ships in the Singapore Strait. The necessity of having cloud context imagery when measuring nighttime lights is made plain by images such as these. The moon was at 67.9° elevation, 188.2° azimuth and 74% illuminated. Camera settings were LWIR high gain, VIS 200msec exposure, SWIR

low-gain 32msec exposure. The nightlights pattern map the growth of the greater Singapore region in Malaysia to the north and in Indonesia's Batam island to the south.

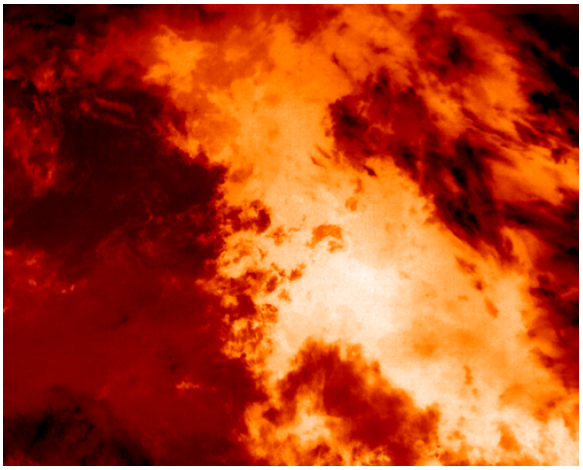

Figure 17. Singapore Imaged by the CUMULOS LWIR microbolometer 2018 Sept. 19, 13:12 UT

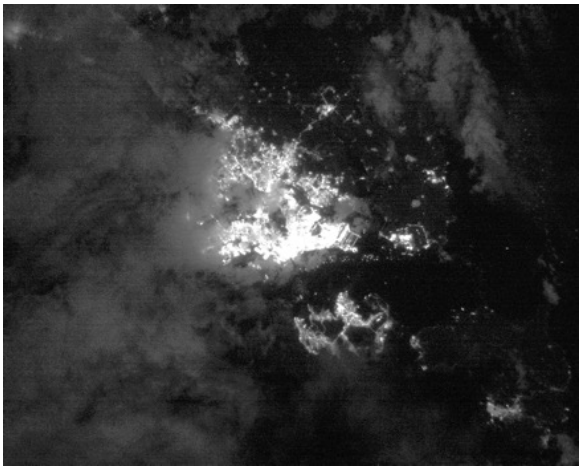

Figure 18. Singapore Imaged by the CUMULOS VIS camera 2018 Sept. 19, 13:12 UT stretched to show moonlit clouds and boats in the Singapore Strait.

Figure 19. Map of the Singapore region.

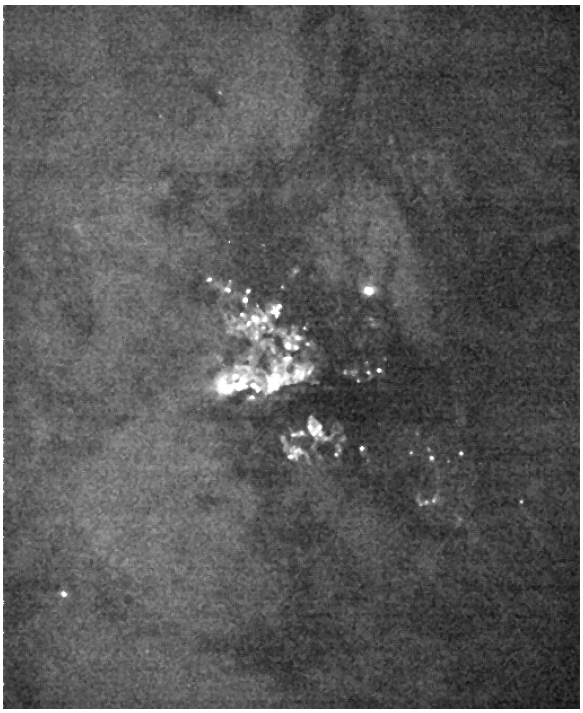

Figure 20. The Singapore region imaged by the CUMULOS SWIR camera 2018 Sept. 19, 13:12 UT.

Jakarta - Airglow Cloud Imaging, No Moonlight

An effort to take new moon images was made early in the CUMULOS flight experiment campaign in order to determine if the 0.9-1.7 micron SWIR camera could image clouds using only airglow illumination.[28] VIIRS has observed this phenomenon, weakly in the DNB. We wanted to use our tiny infrared camera to demonstrate and study the same capability in CubeSat form, by choosing to image in the spectral region where the OH airglow Meinel band emissions peak. There is interest in pursuing such studies to see if the SWIR airglow bands can provide an alternative method for detecting warm clouds such as fog that are difficult to see in the MWIR and LWIR due to low thermal contrast. Our results to date suggest that while this may be possible over ocean regions, low cloud-to-land contrast in our wide open SWIR band, may make cloud discrimination more difficult, generally. The Aerospace Corporation is flying a larger, more capable sensor, the Near InfraRed Airglow Camera (NIRAC) which has just begun operations on the International Space Station, to study all aspects airglow phenomenology in more detail.[29]

Figure 21. shows the SWIR camera Jakarta region image taken at 32msec exposure in high gain mode. The superimposed box approximates the region imaged by the LWIR & VIS cameras. The Jakarta images show a great deal of phenomenology, offshore gas flare signals, saturated city lights partially obscured by clouds, even a

SWIR hotspot from the active volcano Krakatoa at the bottom of the image. Figure 22 show the corresponding LWIR and VIS images of the smaller central region around the Indonesian capital. We are able to demonstrate airglow imaging of clouds by the SWIR camera through comparison to these images. Cloud features seen in the LWIR are clearly also seen in the SWIR image. The VIS camera sees unobstructed off-shore gas flares and city lights made blurry by intervening clouds, but no clouds at all. Moonset was 09:02 UT. Moonrise was 21:54 UT. The lunar phase was 4% waning crescent, and at 15:55UT there was definitively no moonlight in these scenes.

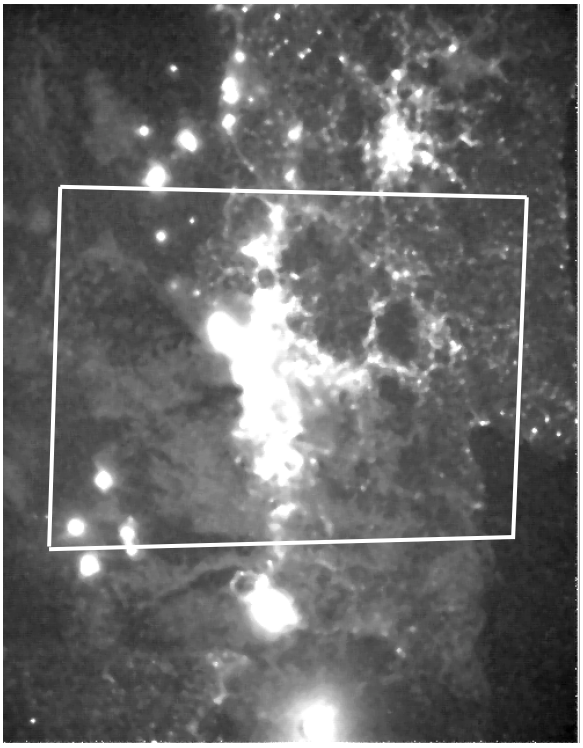

Figure 21. Jakarta and West Java region imaged by the CUMULOS SWIR camera 2018 Jul. 11, 15:55 UT.

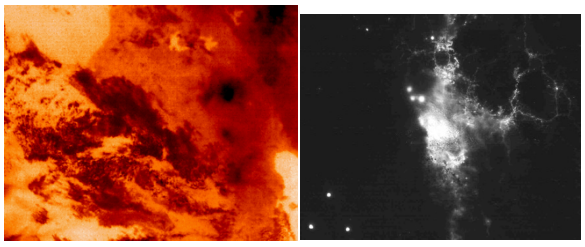

Figure 22. Jakarta region imaged by the CUMULOS LWIR and VIS cameras 2018 Jul. 11, 15:55 UT.

A map of the region turned into the frame of reference of the CUMULOS cameras is shown in Figure 23 for context. This map also plots VIIRS-detected on and off-shore flares. It is quite helpful to have these kinds of known static sources when comparing multispectral imagery.

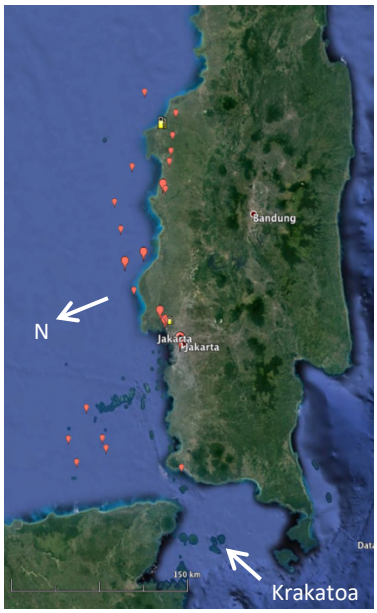

Figure 23. Map of the Jakarta West Java region rotated into the CUMULOS image frame of reference.

CUMULOS - VIIRS Conjunction, Zero Moonlight

A series of CUMULOS and VIIRS conjunction collects have been performed. One goal was comparing airglow imaging of clouds from the CUMULOS SWIR sensor to the VIIRS DNB. One such collect was taken over South Australia in the vicinity of Witjira National Park. The scenes are rather featureless except for a bank of clouds that clearly appear in the LWIR data and which are also barely seen VIIRS DNB and the CUMULOS SWIR camera. The CUMULOS VIS camera sees nothing, as the airglow signal is well below its detection threshold. Figure 24 and 25 show the CUMULOS SWIR and LWIR data, and the VIIRS DNB and CUMULOS VIS data, respectively. The median cloud DNB signal is 0.14 nW-cm^{-1}-sr^{-1}, right at the edge of detectability for this sensor (non-cloud data values were ~0.1 nW-cm^{-1}-sr^{-1}).[30] The CUMULOS SWIR camera data was taken in an autogain mode for which radiometry is not recoverable. Other SWIR frames were taken in programmed modes for which radiometry is possible. These data haven't been successfully reduced yet to extract the calibrated signals which are less distinct than those in the autogain mode image. It is remarkable that the tiny SWIR night vision camera on CUMULOS can detect these weak signals at all with 32msec exposures. Longer exposures would exhibit higher quality imagery. The airglow signal is the combination of direct to space airglow photons as well

as those reflected from the clouds and ground. Taking zero moonlight conjunctions over ocean areas may allow for more straightforward, higher contrast images for comparing VIIRS and CUMULOS results.

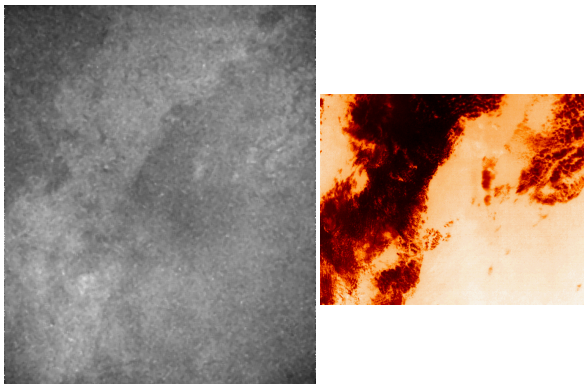

Figure 24. CUMULOS SWIR and LWIR cloud images over Witjira Australia 2018 Dec. 11, 16:02 UT

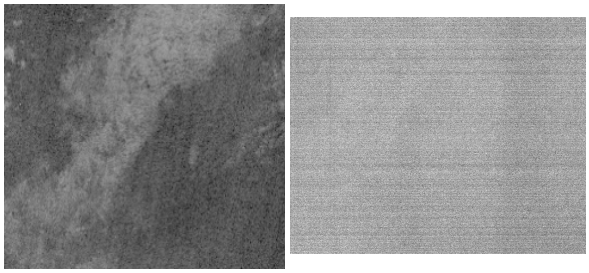

Figure 25. VIIRS DNB and CUMULOS VIS camera cloud images over Witjira Australia 2018 Dec. 11, 16:02 UT. DNB signal is ~ 0.14 nW-cm^{-2}-sr^{-1}.

Hurricane Willa - Twilight Imaging of a Hurricane

CUMULOS was programmed to capture snapshots of the eye of Hurricane Willa off the western coast of Mexico on 23 October, 2018. We wanted to test the microbolometer performance on the highest coldest clouds possible and tropical cyclones are good candidates. The overpass also occurred right after local sunset and over 40 minutes after the last visible geosynchronous image was taken from GOES. Hurricane Willa was reported as a 150 mph, 933 mb category 4 hurricane just before these images were taken. GOES-15 measured brightness temperatures below 60°C in the eye region. Figure 26 shows a LWIR high gain image of the storm center. The sensor is still able to discern cloud structure. This is the coldest Earth-pointed scene the microbolometer has imaged. The 14-bit microbolometer was registering 690 DN on the coldest cloud region. To compare, cold space registers at approximately 620 DN. The microbolometer was losing the ability to subtract its self-emission and detect scene temperature at these levels. GOES measured temperatures below 200K at the same location as depicted in Figure 26, so our microbolometer is running out of signal-to-noise at approximately 200K in accord with tests in TVAC on the ground.[2] The comparison between the microbolometer data and the twilight VIS camera data shows we're still detecting some valid cloud structure with a microbolometer at these very low cold cloud signal levels. Until issues involving the microbolometer signal offsets are studied further, we're not in a position to perform detailed atmospheric profile modeling and temperature extraction from the CUMULOS microbolometer, but we are gathering data on calibration sites such as Lake Tahoe, as discussed in the following section to further explore its on-orbit capabilities and attempt to better quantify them. Figure 27 shows the CUMULOS VIS camera image. The hurricane eye region cloud structure barely imaged by the microbolometer is clearly seen in this post local sunset image.

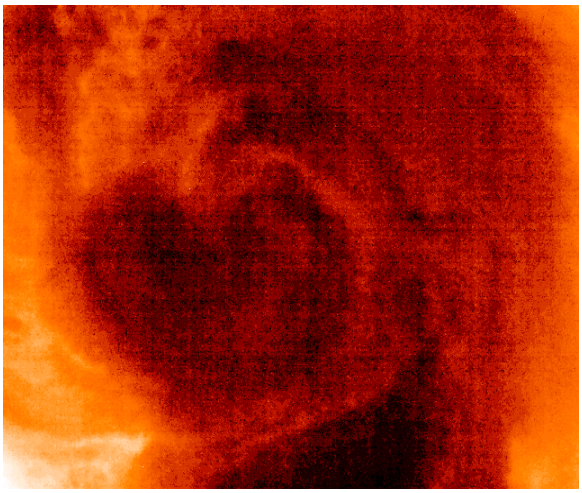

Figure 26. CUMULOS LWIR camera images Hurricane Willa 2018 Oct 23, 01:10:36.24 UT

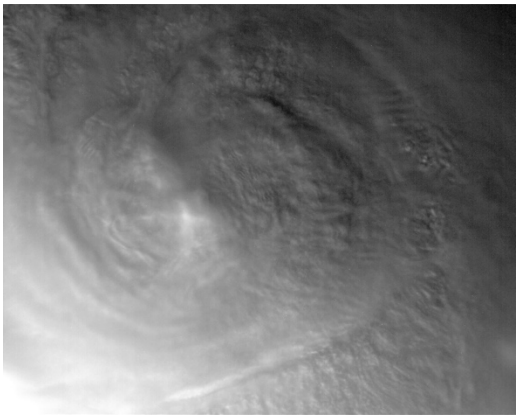

Figure 27. CUMULOS VIS camera images Hurricane Willa 2018 Oct 23, 01:10:47 UT

We used the forecast position of the eye to task the pointing of the CUMULOS cameras to get imagery of the highest, coldest portion of the storm. Figure 28 shows GOES 15 thermal imagery product near the time of the CUMULOS data collection and maps the location of the storm.[31]

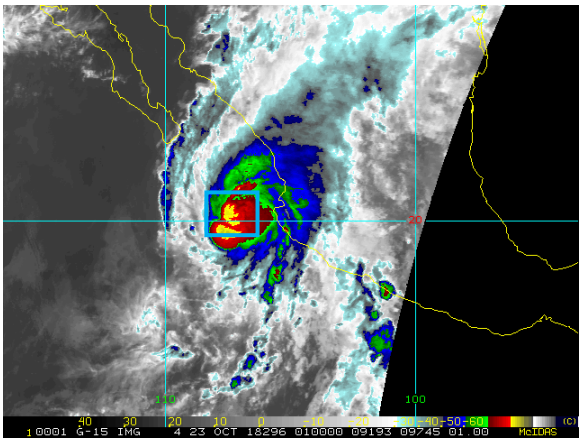

Figure 28. GOES 15 thermal image of Hurricane Willa 2018 Oct 23, 01:15 UT. Blue box outlines the approximate CUMULOS snapshot region.

Daytime Imaging of Thermal Cal Target - Lake Tahoe

Periodically imaging Lake Tahoe under daytime and nighttime conditions for microbolometer calibration studies is an ongoing CUMULOS experiment. Figure 29 shows a largely cloud-free image of the Lake Tahoe region. The CUMULOS VIS and SWIR cameras saturate under many daylight illumination conditions, but can take good early morning and late evening imagery of Earth scenes. The snow covered Sierras appear in this early morning imagery. The SWIR camera shows strong land, water, cloud contrast (with clouds most noticeable in the southwest corner of the image), but no enhanced reflectance from snow. The thermal imagery from the microbolometer highlights temperature differences from the terrain features and highlights Lake Tahoe as a large uniform feature, particularly at the lake's instrumented northern end.

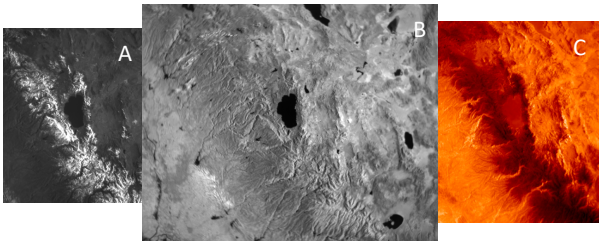

Figure 29. CUMULOS images the Lake Tahoe region on 2019 Apr. 29, 15:40 UT. A)VIS, B) SWIR, C) LWIR

Other daytime imaging data sets have been taken of snowy terrain showing generally similar results, including Mongolia (in conjunction with VIIRS), far eastern Russia, and the Mt. Everest region in the Himalayas. These data are also being used for testing our automated georegistering data pipeline.

DISCUSSION AND CONCLUSIONS

CUMULOS was built and tested rapidly to respond to an opportunity to insert a secondary payload on the NASA/JPL ISARA mission. The 3-camera design targeted several "VIIRS-like" missions and has served as a pathfinder for our CubeSat operations and data pipelining efforts. The CUMULOS program has demonstrated several unique contributions during its first year on orbit: stellar calibration techniques, new mission capabilities, and infrared sensor performance in space. These are summarized below.

Calibration

The CUMULOS project demonstrated the use of bright stars for on-orbit calibration of CubeSat sensors. This technique is suited for radiometrically calibrating the detection of nighttime signals emitted by artificial lighting, fires and gas flares and, if used carefully, can be used to understand the signal levels of moonlit or airglow-illuminated clouds. Other calibration demonstrations are still to be completed, notably implementing the ROLO model using the moon as a VIS and SWIR calibration source, and assessing the performance of the microbolometer through vicarious calibration via VIIRS conjunctions and via modeling and reducing observations of well instrumented thermal calibration sites such as Lake Tahoe.

High Resolution Calibrated Nighttime Lights

The CUMULOS VIS camera has produced a number of cloud-free observations of major metropolitan areas at 5.6 times higher resolution than the VIIRS DNB. These data can be used to better understand the urban geography, light pollution, energy usage, infrastructure and transportation grids of the studied regions. It is our goal to release these data for general use. In addition to urban areas, experimental observations have been made of gas flare regions, boat concentrations and other phenomena of general interest to nightlights researchers. The SWIR and LWIR data add to the usefulness of these data sets.

SWIR Airglow-Illuminated Cloud Imagery

The CUMULOS SWIR camera successfully demonstrated imaging of clouds at night in the absence of moonlight, a new approach to the original DMSP OLS and VIIRS DNB mission. By operating in the 0.9-1.7 micron band where the OH airglow Meinel bands peak, we demonstrated that a tiny camera can detect airglow illuminated cloud and land surfaces. These data will be

assessed for weather imaging utility, and will be used jointly with the newly operational ISS-based Near InfraRed Airglow Camera (NIRAC) in an effort to better understand the meteorological applications of airglow phenomenology.[29]

LWIR Microbolometer Utility and Weather Imaging

The CUMULOS program launched the first microbolometer successfully operated in space on a CubeSat. Despite the challenges presented by the orbital thermal environment, the CUMULOS microbolometer has reliably produced clean interpretable thermal cloud context, terrain imagery and hotspot data. Additional work is in progress to fully assess the performance of this FLIR Sys. wide-bandwidth LWIR camera. Performance for cloud imaging degraded at about 200K, in accord with our ground test data. This doesn't impact the utility of the camera for qualitative cloud cover imaging.

CubeSat Fire Mission Capability

The CUMULOS program demonstrated nighttime capability for mapping fire perimeters and hotspots via a low-cost three camera VIS, SWIR, LWIR remote sensing system. Performance of the VIS and SWIR sensors was excellent, and produced results comparable to large satellites such as VIIRS and MODIS over the modest field of view of the CUMULOS cameras.[26] The microbolometer also performed quite well. An operational CubeSat fire mission should have a somewhat higher resolutions if the LWIR is to be used as the primary daytime fire detection sensor, rather than as a cloud context and thermal context imager. This is necessary to increase performance to sub-pixel sized fire lines. Exploring compact MWIR sensors is a goal for a follow-on sensor to CUMULOS.

Acknowledgments

This research was funded by The Aerospace Corporation's Independent Research and Development program.

References

1. Pack, D.W., Ardila, D.R., Herman, E., Rowen, D. W., Welle, R.P., Wiktorowicz, S.J., and Hattersley, B.W., "Two Aerospace Corporation CubeSat Remote Sensing Imagers: CUMULOS and R3", Proceedings of the AIAA/USU Conference on Small Satellites, CubeSat Session 3,SSC17-III-05.2017. https://digitalcommons.usu.edu/smallsat/2017/all2017/82/

2. Ardila, D.R., Pack, D.W., "The Cubesat Multispectral Observing System (CUMULOS)." Conference on Characterization and Radiometric Calibration for Remote Sensing, (2016). https://digitalcommons.usu.edu/calcon/CALCON2016/all2016content/27/

3. Elvidge, C. D., Ziskin, D., Baugh, K. E., Tuttle, B. T., Ghosh, T., Pack, D. W., Erwin, E. H., Zhizhin, M., "A Fifteen Year Record of Global Natural Gas Flaring Derived from Satellite Data", Energies, vol.2, no. 3, 2009.

4. Miller, S.D, Mill, S.P., Elvidge, C.D., Lindsey, D. T., Lee, T.F., Hawkins, J.D., "Suomi Satellite Brings to Light a Unique Frontier of Nighttime Environmental Sensing Capabilities", Proceedings of the National Academy of Sciences, vol. 109, no. 39, September, 2012.

5. Miller, S.D., Straka III, W., Mills, S., Elvidge, C., Lee, T., Solbrig, J., Walther, A., Heidinger, A., Weiss, S., "Illuminating the Capabilities of the Suomi National Polar-Orbiting Partnership (NPP) Visible Infrared Imaging Radiometer Suite (VIIRS) Day/Night Band", Remote Sensing, vol. 5, 2013.

6. Katayama, H., Sakai M., Kato, E., Nakajima, Y., Nakau, K., and Kimura, T., "On-orbit performance of the Compact Infrared Camera (CIRC) with uncooled infrared detector", Proc. SPIE 9451, Infrared Technology and Applications XLI, 94511D, 2015.

7. Pack, D.W., Hardy, B.S. "CubeSat Nighttime Lights" Proceedings of the AIAA/USU Conference on Small Satellites, CubeSat Session IV: LEO Missions, SSC16-WK-44. 2016. http://digitalcommons.usu.edu/smallsat/2016/S4LEOMis/1/

8. Pack, D. W., Hardy, B. S., Longcore, T., "Studying the Earth at Night from CubeSats", Proceedings of the AIAA/USU Conference on Small Satellites, CubeSat Session 10, SSC17, SSC17-WK-35,2017. https://digitalcommons.usu.edu/smallsat/2017/all2017/41/

9. Pack, D.W., Hardy, B.S. "CubeSat Nighttime Earth Observations", AGU 2017 Fall Meeting - https://agu.confex.com/agu/fm17/meetingapp.cgi/Paper/245666

10. Rudy, R. J. 2007, "Models of Stellar Spectral Energy Distributions for the Optical and Infrared", Aerospace Technical Report ATR-2007(8189)-1.

11. Russell, R., Rudy, R., Wiktorowicz, S., Rossano, G., Mauerhan, J., Subasavage, J., Kim, D., Crawford, K., Gutierrez, D, and Owens, M. Proceedings, "The Aerospace Spectral Energy Distribution (ASED) Program: 2018 Update",

Conference on Characterization and Radiometric Calibration for Remote Sensing, Space Dynamics Laboratory, Logan Utah June 20, 2018. https://digitalcommons.usu.edu/calcon/CALCON2018/all2018content/21/

12. Yoon, H.W. and Kacker, R.N., "Guidelines for Radiometric Calibration of Electro-Optical Instruments for Remote Sensing", NIST HB 157 National Institute of Standards and Technology: Gaithersburg, MD, USA, 2015. http://dx.doi.org/10.6028/NIST.HB.157

13. Kieffer, H. H., and Stone, T. C. , The Spectral Irradiance of the Moon, The Astronomical Journal **129**, 2887–2901, 2005.

14. Stone, T.C., "Using the Moon as a Common Reference for Intercalibration", Conference on Characterization and Radiometric Calibration for Remote Sensing, Space Dynamics Laboratory, Logan Utah 22-25 August 2016. https://digitalcommons.usu.edu/calcon/CALCON2016/all2016content/20/

15. Landsat calibration activities and research and test sites are catalogued at: https://www.usgs.gov/land-resources/eros/calval, with the test site catalog available at: https://calval.cr.usgs.gov/apps/test_sites_catalog

16. Lake Tahoe test data from a joint JPL/UC Davis project dating to 1999 is catalogued at: https://laketahoe.jpl.nasa.gov/

17. Elvidge, Christopher D., Mikhail Zhizhin, Feng-Chi Hsu, and Kimberly E. Baugh. "VIIRS nightfire: Satellite pyrometry at night." Remote Sensing 5, no. 9, 4423-4449, 2013.

18. Elvidge, C.D, Zhizhin, M., Baugh, K., Hsu, F.-C., Ghosh, T., "Methods for Global Survey of Natural Gas Flaring from Visible Infrared Imaging Radiometer Suite Data", Energies, vol. 9, January 2016.

19. Elvidge, C.D.; Zhizhin, M.; Baugh, K.; Hsu, F.-C. Automatic Boat Identification System for VIIRS Low Light Imaging Data. *Remote Sens.*, *7*, 3020-3036. 2015.

20. Welle, R.P. Coffman, C.M., Pack, D.W. John R. Santiago, J.R., "CubeSat Laser Communication Crosslink Pointing Demonstration", Proceedings of the AIAA/USU Conference on Small Satellites, 2019. Reference number SSC19-VI-06

21. Personal communication, Richard J. Rudy, also see reference 10.

22. Elvidge, C.D, Cinzano, P., Pettit, D.R., Arvesen, J., Sutton, P., Small, C., Nemani, R., Longcore, T., Rich, C., Safran, J., Weeks, J, Ebener, S. "The Nightsat Mission Concept", International Journal of Remote Sensing, vol. 28, No. 12, May 2007.

23. Kyba, C.C.M., Garz, S. Kuechly, H., De Miguel, S.A., Zamorano, J., Fischer, J., Hölker, F., "High-Resolution Imagery of Earth at Night: New Sources, Opportunities and Challenges", Remote Sensing, vol. 7, 1-23, January 2015.

24. De Miguel, S.A.; Castaño, J.G.; Zamorano, J.; Kyba, C.C.M.; Pascual, S.; Ángeles, M.; Cayuela, L.; Martin Martinez, G.; Caltner, P., "Atlas of astronaut photos of Earth at night" Astronomy and Geophysics, vol. 55, no. 4 August 2014. This helpful Atlas to nighttime ISS photography is described by Kyba et. al. in reference 23 and online at: http://www.citiesatnight.org, and http://www.nightcitiesiss.org/

25. CUMULOS results were compared to MODIS fire products produced by ESRI (Earth Science Research Institute).

26. Pack, D.W., Coffman, C.M., Rowen, D.W., Santiago, J.R., Kinum, G., and Russell, R.W., "Earth Remote Sensing Results from the CUbesat MULtispectral Observing System, CUMULOS", AGU Fall Meeting 2018, https://agu.confex.com/data/handout/agu/fm18/Paper_457011_handout_16889_0.pdf

27. Elvidge, C., Ghosh, T., Baugh, K., Zhizhin, M., Hsu, F., Katada, N., Penalosa, W. and Hung, Q. "Rating the Effectiveness of Fishery Closures With Visible Infrared Imaging Radiometer Suite Boat Detection Data", Front. Mar. Sci. v.5 April 2018.

28. Pack, D.W., Coffman, C.M., Rowen, D.W., Santiago, J. Russell, R.W., Kinum, G., Hardy, B.S. Welle, R.P., Venturini, C. C., "CUMULOS: Early On-orbit Imaging Results", Proceedings of the AIAA/USU Conference on Small Satellites, 2018. https://digitalcommons.usu.edu/smallsat/2018/all2018/362/ https://digitalcommons.usu.edu/cgi/viewcontent.cgi?filename=0&article=4174&context=smallsat&type=additional

29. Rudy, R., Gelinas, L., Hecht, J., "NIRAC: Near Infrared Airglow Camera for the International Space Station", AGU Fall Meeting 2017.

30. Personal communication, Steven D. Miller.

31. Tropical cyclone data from the 2018 season is archived by CIRA at: http://rammb.cira.colostate.edu/products/tc_realtime/season.asp?storm_season=2018